

# AN EMBEDDED ZONAL LES METHOD APPLIED FOR PREDICTIONS IN TURBOMACHINERY APPLICATIONS

*J. Borgelt<sup>1</sup>, M. Meinke<sup>1</sup>, W. Schröder<sup>1,2</sup> and D. Krug<sup>1,2</sup>*

<sup>1</sup> *Institute of Aerodynamics and Chair of Fluid Mechanics (AIA), RWTH Aachen University*

<sup>2</sup> *JARA Center for Simulation and Data Science, Jülich, Germany*

*j.borgelt@aia.rwth-aachen.de*

## Abstract

An embedded LES (ELES) method is introduced which combines the efficiency of Reynolds-averaged Navier-Stokes (RANS) models with the turbulence-resolving capabilities of large-eddy simulation (LES) for turbomachinery flows. The embedded LES method is applied to a generic axial turbine geometry to predict the sealing efficiency of the rim seal and the hot gas ingress into the wheel space with higher accuracy compared to a RANS method. The flow region in which the ELES is performed is limited to the vicinity of the rim seal gap and the wheel space to minimize the computational cost. At the inflow boundary of the ELES region, a synthetic turbulence generation method is used, which also allows the introduction of freestream turbulence. At the domain boundary, which is almost tangential to the main flow direction, the mass flux determined by the preliminary RANS is defined. Navier-Stokes characteristic boundary conditions are formulated at the outflow boundary. To assess the accuracy of the ELES and RANS, a full LES is performed as a reference solution. The comparison of the results shows that the RANS method predicts the flow field in the main flow passage in good agreement with the full LES, but does not accurately predict the hot gas ingress. The ELES results are almost identical to the full LES for the main flow passage and the hot gas ingress at 60% of the computational cost of the full LES.

## 1 Introduction

Improving the thermal efficiency of turbomachinery can substantially reduce the emission of pollutants and the amount of fossil energy used by the transport and energy sector. An important parameter for the thermodynamic efficiency is the turbine inlet temperature. The higher thermal loads due to the increased temperature, however, result in immense challenges in the design of the turbine cooling system, which is needed to increase the safety and lifetime of the turbine stages. Hot gas from the outer main annulus flow can enter the wheel space through the rim seal gap, which leads to high thermal loads and possibly to material damage, which must be avoided. To prevent the ingress of main annulus gas into the wheel space, sealing air from the turbine's secondary air system is in-

roduced into the wheel space. Since higher sealing air mass flow result in a reduced machine efficiency, sophisticated rim seal geometries are developed to minimize the necessary amount of sealing air.

The intricate interaction of rotation driven and multi-mode ingress involving turbulent shear layers is difficult to capture accurately by solutions of the Reynolds averaged Navier-Stokes (RANS) equations, see Horwood et al. (2019). Previous work has shown that an accurate prediction of the hot gas ingress into the wheel space can be obtained using higher fidelity turbulence modeling, in which the inertial part of the turbulence spectrum is resolved, i.e., large-eddy simulations (LES). However, the significantly improved quality of the numerical results based on LES is associated with a considerably higher computational cost. To combine the computational efficiency of RANS and the accuracy of LES, an embedded LES (ELES) method is presented to simulate the unsteady hot gas ingress in a simplified generic turbine geometry. The region of interest is reduced to areas where resolutions beyond the integral length scale are necessary, i.e., the rim seal gap.

The paper is structured as follows. First, the numerical discretization is described. Then, the embedded LES method is discussed and changes from the original embedded LES method by Borgelt et al. (2025) are highlighted. Subsequently, the embedded LES method is applied to a simplified axial turbine setup and the results are discussed by comparing the findings of the ELES with the solution of a full RANS and LES simulation.

## 2 Numerical method

The multi-physics solver m-AIA (multiphysics-Aerodynamisches Institut Aachen) developed at the Institute of Aerodynamics, RWTH Aachen University (2024) is utilized for this study.

The simulation framework employs a finite-volume and a level-set solver, both designed for adaptively refined Cartesian meshes. These solvers are tightly coupled by managing individual subsets of the shared hierarchical mesh.

The finite-volume method solves the conservation equations for a viscous, compressible fluid. In the LES formulation, the turbulent structures down to the inertial subrange are resolved. The sub-grid scale (SGS)

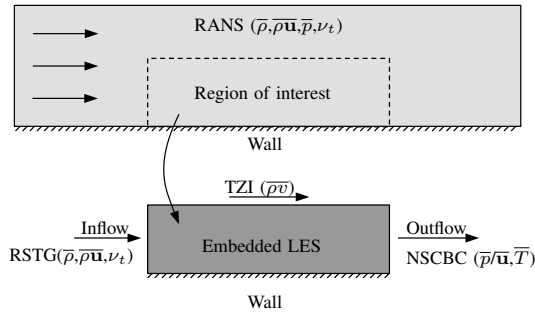


Figure 1: Schematic of the embedded LES with the different interfaces inside the surrounding RANS domain, Borgelt et al. (2025)

contributions are modeled using the monotone integrated LES (MILES) approach with an implicit filter. The numerical discretization of the inviscid and viscous fluxes and the time integration is described in more detail in Schneiders et al. (2016).

In the RANS approach, the Fares-Schröder turbulence model by Fares and Schröder (2005) is used to calculate the Reynolds stresses.

A strictly conservative cut-cell approach is employed to accurately capture the geometry of embedded bodies, whose surfaces are defined by the zero level-set contour generated by the level-set solver. To mitigate the restriction of excessively small time steps in regions with small cut-cells, a flux redistribution technique is applied. Comprehensive details of the cut-cell formulation and the associated flux redistribution strategy are provided in Schneiders et al. (2016).

### 3 Embedded LES method

The embedded LES method by Borgelt et al. (2025) is applied to turbomachinery flow. The Navier-Stokes characteristic boundary condition (NSCBC) presented in Borgelt et al. (2025) is used at the outflow of the embedded LES domain. The boundary condition uses the pressure field for positive streamwise velocities and the density and velocity field for negative streamwise velocities of a preliminary RANS encompassing the full domain to prescribe meaningful target values for the incoming and outgoing characteristics. A tangential zonal interface (TZI), see Borgelt et al. (2025), allows the correct mass flux to enter or leave the embedded LES domain over a surface approximately tangential to the velocity field. At the inflow of the LES domain, the reformulated synthetic turbulence generation (RSTG) method by Roidl et al. (2013), that has been adapted to allow for the generation of freestream turbulence, is used to generate turbulent velocity fluctuations from the time averaged values of the preliminary RANS solution. Figure 1 schematically shows the three interfaces of the embedded LES region and the information from the RANS used to define the boundary conditions.

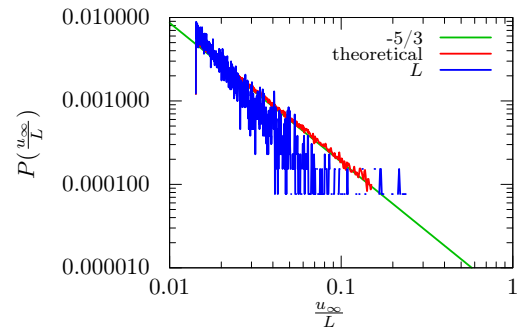


Figure 2: Power density function of the freestream eddy size  $u_\infty/L$ .

### Extension of the synthetic turbulence method for freestream turbulence

To efficiently simulate flow in turbomachinery applications, the synthetic turbulence generation method is extended to include freestream turbulence. This extension is particularly important due to its influence on boundary layer separation on the stator blade, which in turn significantly affects the pressure distribution on the blade surfaces and the resulting hot gas ingress.

To capture these effects, the generation of synthetic eddies has been extended to span the entire inflow plane of the embedded LES region. The eddy size distribution for freestream turbulence is determined using a scaling law based on a cumulative distribution function given by

$$L_{scaling} = \left(\frac{m+1}{c} \cdot r\right)^{1/(m+1)} \quad (1)$$

where  $m = 5/3$  corresponds to the inertial range of the turbulence spectrum,  $r \in [0, 1]$  is a uniformly distributed random number, and  $c$  is a geometry-dependent constant such that the maximum eddy size is approximately half the channel height.

The actual eddy size  $L$  is

$$L = L_{scaling} \cdot \delta_{99}, \quad (2)$$

where  $\delta_{99}$  is the boundary layer thickness at the inflow plane. The resulting probability density function (PDF) of the eddy sizes is illustrated in Figure 2. The theoretical probability distribution from Equation (1) is compared with the numerical probability distribution of the eddy size  $P(u_\infty/L)$  obtained from 40 sampled time steps. The numerical eddy size distribution closely aligns with the theoretical probability distribution, with the exception of small eddy sizes, where deviations arise due to the breakdown of the law of large numbers.

### 4 Numerical setup

A simplified axial turbine setup with a generic stator based on a NACA9420 profile is used to test the embedded LES method. Figure 3 shows the simplified turbine geometry with the embedded LES region,

Table 1: Operating conditions for the simplified turbine geometry.

Reynolds number main flow	$Re_{hg} = \frac{\rho_{hg} c_{hg} R}{\mu_{hg}} = 0.405 \cdot 10^6$
Mach number main flow	$Ma_{c1} = \frac{c_1}{a_1} = 0.15$
Rotational Reynolds number	$Re_u = \frac{\rho_{hg} \Omega R^2}{\mu_{hg}} = 0.324 \cdot 10^6$
Dimensionless sealing air mass flux	$c_w = \frac{\rho_{cg} u_{cg} A_{cg}}{\mu_{cg} R} = 425$

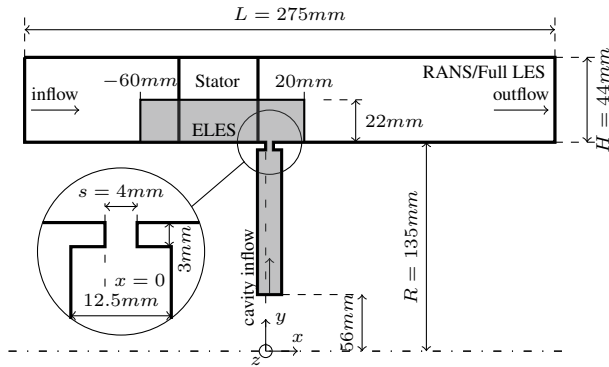


Figure 3: Schematic of the simplified turbine geometry with the location of the embedded LES (ELES) region.

which encompasses the turbulent boundary layer upstream of the stator, part of the stator blade, and the wheel space. The stator creates a flow deflection of  $36^\circ$  in the  $z$ -direction, in which a periodic boundary condition is used. The geometry of the wheel space and rim-seal gap is based on the ICAS-GT2 turbine geometry investigated by Jakoby et al. (2004) and Hösgen et al. (2023,2024). The hub radius of the rotor is  $R = 135\text{mm}$  and the height of the main annulus is  $H = 44\text{mm}$ . The length of the main annulus is  $L = 275\text{mm}$ . The extent of the seal gap in the streamwise direction  $x$  is  $s = 4\text{mm}$ . The wheel-space is symmetric with a double lip geometry.

The operating conditions of the simplified turbine geometry are summarized in Table 1.

## 5 Computational grid

The number of grid cells for the different simulations are summarized in table 2. The grid of the pure LES and pure RANS setup consists of 175 million cells. The zonal setup has a grid size of 70 million cells, corresponding to a reduction in grid cells of 60%. Figure 4 shows the Cartesian grid of the embedded LES region.

Table 2: Number of cells of the different setups.

setup	RANS	LES	ELES
grid cells [ $10^6$ ]	175	175	70

## 6 Results

In the following, the reformulated embedded LES (ELES) methodology is validated. The performance of the ELES approach is evaluated against fully re-

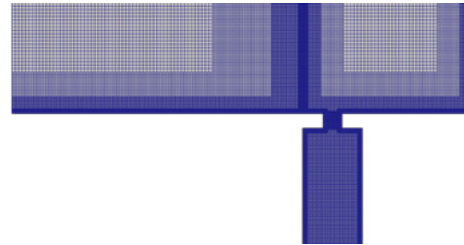


Figure 4: Cartesian grid of the embedded LES region in the plane  $z = 0$ . Only the upper part of the wheel space refinement is shown.

solved LES and preliminary RANS simulations to assess the accuracy and computational efficiency of the ELES method, particularly in capturing the cooling effectiveness of the rim seal region.

First, the main annulus flow is analyzed, focusing on velocity and pressure distributions across the different simulation approaches. Particular attention is paid to the influence of modeled freestream turbulence by comparing ELES simulations with (ELES) and without (ELESnFS) synthetic turbulence generation to the reference LES results.

Subsequently, the cavity flow is analyzed in terms of integral quantities such as mass ingress rates and time and spanwise averaged flow fields within the wheel space. Key metrics include the spatial distribution of cooling effectiveness and Reynolds stress components associated with hot gas ingress. The comparisons provide a comprehensive evaluation of each simulation method's ability to capture the dominant physical mechanisms determining the cavity sealing performance.

### Main channel flow

Figure 5 presents an instantaneous visualization of the Q-criterion, colored by velocity magnitude, within the embedded LES region. This highlights key turbulent features including the stator wake, the development of a turbulent boundary layer along the annulus wall, and the interaction of the boundary layer with the shear layer emerging from the rim seal gap.

Figure 6 displays the time averaged streamwise velocity component  $u_m$  at a normalized radial height of  $y/R = 1.08$ , that corresponds to the midplane of the main annulus in the embedded LES region. The comparison between the different simulation approaches reveals notable differences in the resolution of the stator wake. The steady RANS simulation shows good

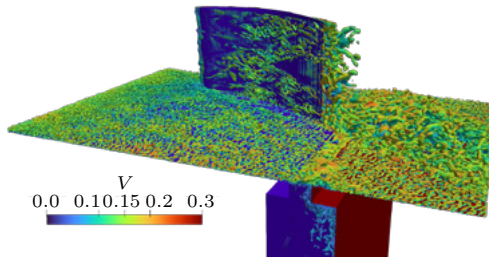


Figure 5: Q-criterion colored by the instantaneous velocity magnitude  $V$  of the embedded LES region. The stator wall is colored in blue, the rotor wall in red.

agreement in the flow field upstream of the stator trailing edge. However, it underpredicts the size of the recirculation region downstream of the stator compared to the reference LES.

The embedded LES simulation without prescribed freestream turbulence (ELESnFS) exhibits a significantly larger recirculation region compared to both the ELES configuration with prescribed freestream turbulence and the pure LES. This discrepancy is attributed to the missing turbulent structures in the inflow in the ELESnFS case, which leads to earlier boundary layer separation and an inability of the flow to remain attached along the stator curvature. Note, that streamwise extent of the inlet and outlet planes of the ELESnFS case are slightly larger than in the ELES setup. The current observations are consistent with findings reported for laminar inflow conditions over wind turbine blades by Huang et al. (2020). The embedded LES simulation with synthetic freestream turbulence shows good quantitative agreement with the fully resolved LES in terms of wake structure and flow reattachment. This underlines the importance of appropriate turbulence generation at the ELES-RANS interface to accurately capture the main channel flow behavior.

To quantify the differences between the varying simulation methods, the time averaged pressure coefficient  $c_p$  at  $y/R = 1.08$ , located mid-span in the main annulus of the embedded LES domain, is shown in figure 7. The distributions observed there for the ELESnFS case confirm the previous discussion.

Figure 8 presents the time averaged wall-shear stress  $\tau_w$  at  $z/s = -4.75$  along the stator leading edge, with the position of the evaluation line indicated at the bottom of the figure. The RANS solution closely matches the LES results upstream of the stator leading edge. The ELES configuration also aligns well with LES in this region. Unlike the pure RANS, it also shows good agreement with the reference LES downstream of the stator blade. The ELESnFS setup deviates significantly upstream of the rotor and in the stator wake within the enlarged recirculation region. Outside of this region ( $x/s > -4$ ), deviations from the LES are minimal and comparable to those observed with

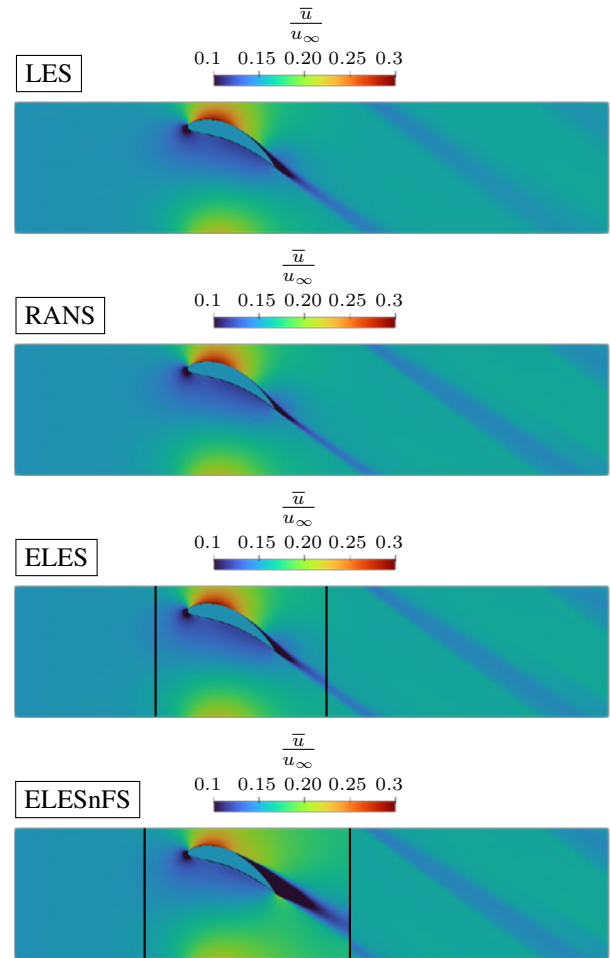


Figure 6: Time average for the streamwise velocity component  $\bar{u}/u_\infty$  in the center plane of the main annulus of the embedded LES domain at  $y/R = 1.08$ . From top to bottom: pure LES, pure RANS, embedded LES (ELES) setup surrounded by the RANS solution, and embedded LES setup without freestream turbulence (ELESnFS) surrounded by the RANS solution. The embedded LES domain is marked by the black solid line in the bottom figures.

the ELES setup.

### Cavity flow

Next, the cavity flow behavior is analyzed. The discussion is divided into two parts: first, the assessment of hot gas ingress based on integral metrics and second, the examination of time and spanwise averaged radial distributions of key flow quantities within the wheel space.

To quantify the sealing performance, the integral sealing effectiveness  $H$

$$H = \int_{V_{ws}} \frac{Y(\mathbf{x}) - Y_{hg}}{Y_{cg} - Y_{hg}} dV, \quad (3)$$

where  $Y$  denotes the passive scalar concentration, with  $Y_{hg} = 0$  and  $Y_{cg} = 1$ ,  $V_{ws}$  is the volume of the

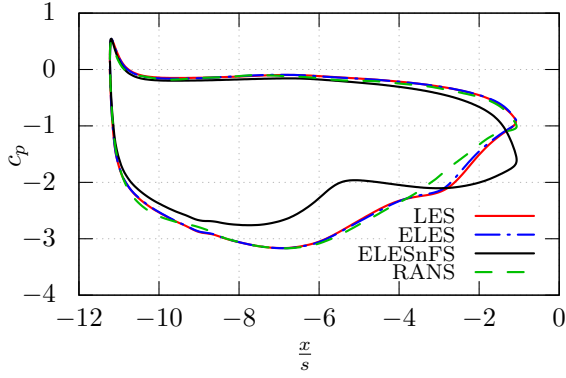


Figure 7: Time averaged pressure coefficient  $c_p$  in the mid-plane of the main annulus of the embedded LES domain at  $y/R = 1.08$ .

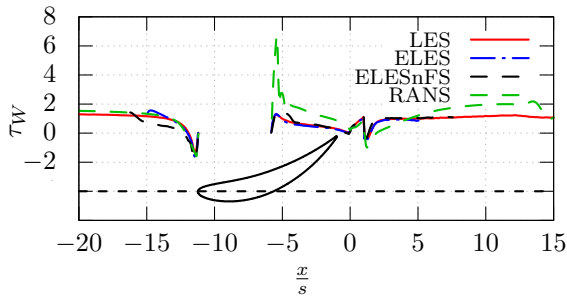


Figure 8: Time averaged wall-shear stress  $\tau_w$  at  $z/s = -4.75$  through the leading edge of the stator.

wheel space, and  $\mathbf{x}$  is the position vector, is considered.

The maximum penetration of hot gas into the cavity is characterized by the minimum radial position  $R_{min}$  at which a concentration threshold

$$R_{min} = \min_{\mathbf{x} \in V_{ws}} \left\{ r \left| \frac{Y(\mathbf{x}) - Y_{hg}}{Y_{cg} - Y_{hg}} > 0.99 \right. \right\} \quad (4)$$

is exceeded.

Table 3 summarizes the values of  $\bar{H}$  and  $R_{min}$  for the different simulation setups. The pure RANS simulation overpredicts the sealing effectiveness. The value  $\bar{H}_{RANS} = 0.924$  is significantly higher than that of the reference LES result  $\bar{H}_{LES} = 0.876$ . The corresponding maximum ingress depth defined by  $R_{min}$  is also lower for the RANS case  $R_{min,RANS} = 0.78$  compared to the LES case  $R_{min,LES} = 0.64$ . The ELES configuration with synthetic freestream turbulence agrees close with the LES. The deviation in  $\bar{H}$  is approx. 0.8% and that in  $R_{min}$  2%. In contrast, the results of ELES configuration without prescribed freestream turbulence (ELESnFS) are similar to the RANS solution which again highlights the necessity to prescribe freestream turbulence.

Figure 9 presents the radial distributions of the

Table 3: Time averaged integral sealing effectiveness  $\bar{H}$  and the maximum penetration  $R_{min}$  for the different simulation setups.

setup	RANS	LES	ELES	ELESnFS
$\bar{H}$	0.924	0.876	0.869	0.953
$R_{min}$	0.78	0.64	0.63	0.75

cooling effectiveness  $\eta$

$$\eta = \frac{Y(y) - Y_{hg}}{Y_{cg} - Y_{hg}} \quad (5)$$

The distributions are shown for three axial positions inside the wheel space. The radial distributions for the wheel-space at  $x/s = -3.75$ , i.e., close to the stator wall, are shown in the left column, the radial distributions in the center of the wheel space at  $x/s = 2.0$  are shown in the middle column, and the radial distributions inside the wheel-space close to the rotor disk at  $x/s = 7.75$  are displayed in the right column. The ELES solutions show good agreement in the sealing effectiveness and the radial velocity distributions compared to the pure LES data.

The radial distributions of the Reynolds stress components relevant for the hot gas ingress, i.e.  $\overline{u'v'}$  and  $\overline{v'v'}$ , are also shown for the three axial positions in figure 9. The Reynolds stresses of the embedded LES setup with prescribed freestream turbulence is found to be in excellent agreement with the pure LES at all positions inside the wheel space and the main annulus in the stator wake. The distributions of the embedded LES setup without prescribed freestream turbulence possesses a significant difference in the Reynolds stress components corresponding to the significantly lower prediction in hot gas ingress.

## 7 Conclusions

The embedded LES (ELES) method by Borgelt et al. (2025) was used to determine the of hot gas ingress in a generic axial gas turbine configuration. The inflow boundary condition was reformulated to generate turbulent flow in the boundary layer and freestream flow. This was essential to correctly capture the stator and ingress flow. The ELES approach, the number of grid cells is reduced by 60% compared to the full LES, showed good agreement with the full LES results. The pure RANS solution showed a significantly higher sealing efficiency with a reduced hot gas ingress compared to the full LES solution.

## Acknowledgments

The authors gratefully acknowledge the Gauss Centre for Supercomputing e.V. ([www.gauss-centre.eu](http://www.gauss-centre.eu)) for funding this project by providing computing time on the GCS Supercomputer HAWK at Höchstleistungsrechenzentrum Stuttgart ([www.hlr.de](http://www.hlr.de)).

The research project was performed in the framework of the industrial collective research programme

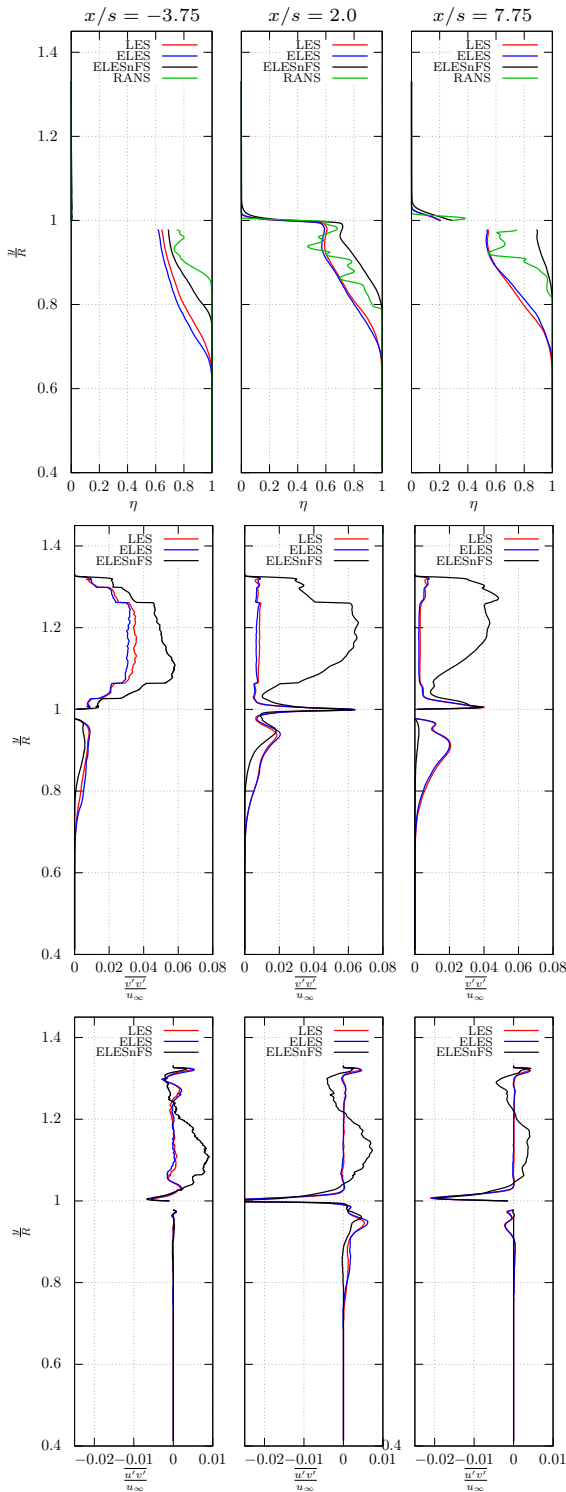


Figure 9: Time and spanwise average for (top) the cooling effectiveness  $\eta$ , (center) the Reynolds normal stress  $\overline{v'v'}$ , and (bottom) Reynolds shear stress  $\overline{u'v'}$  versus radial position  $r$  for (left)  $x/s = -3.75$ , (center)  $x/s = 2.0$ , and (right)  $x/s = 7.75$ .

(IGF No. 20544N). It was supported by the Federal Ministry for Economic Affairs and Energy (BMWi) through the AiF (German Federation of Industrial Re-

search Associations eV) based on a decision taken by the German Bundestag.

The authors gratefully acknowledge the German Federal Ministry of Education and Research (BMBF) and the state government of North Rhine-Westphalia for supporting this work/project as part of the NHR funding.

## References

- Borgelt, J., Meinke, M. and Schröder, W. (2025), Embedded LES boundary conditions for shear dominated flows, *Computers & Fluids*, Vol. 299, pp. 106729, <https://doi.org/10.1016/j.compfluid.2025.106729>.
- Fares, E. and Schröder, W. (2005), A general one-equation turbulence model for free shear and wall-bounded flows, *Flow Turbulence Combust*, Vol. 73, pp. 187–215, <https://doi.org/10.1007/s10494-005-8625-y>.
- Hösgen, T., Meinke, M. and Schröder, W. (2023), Analysis of Single Blade Passage and Full Circumference Large-Eddy Simulations of Turbine Rim Seal Flows. *Journal of Turbomachinery*, Vol. 146. pp. 1-20.
- Horwood, J. T. M., Hualca, F. P., Scobie, J. A., Wilson, M., Sangan, C. M. and Lock, G. D. (2019), Experimental and computational investigation of flow instabilities in turbine rim seals, *J. Eng. Gas Turbines Power*, Vol. 141, pp. 011028.
- Hösgen, T., Meinke, M. and Schröder, W. (2024), Analysis of Ingress Into the Downstream Wheel Space of a 1.5-Stage Turbine By Full Circumference and Single Blade Passage Large-Eddy Simulations. *Journal of Turbomachinery*, Vol. 146. pp. 1-9.
- Huang X., Albers M., Meysonnat P., Meinke M. and Schröder W. (2020), Analysis of the effect of freestream turbulence on dynamic stall of wind turbine blades, *International journal of heat and fluid flow*, Vol. 85, pp. 108668, <https://doi.org/10.1016/j.ijheatfluidflow.2020.108668>.
- Institute of Aerodynamics, RWTH Aachen University (2024), m-AIA, *Zenodo*, <https://doi.org/10.5281/zenodo.13350586>.
- Roidl, B., Meinke and M., Schröder, W. (2013), A reformulated synthetic turbulence generation method for a zonal RANS–LES method and its application to zero-pressure gradient boundary layers, *International Journal of Heat and Fluid Flow*, Vol. 44, pp. 28-40.
- Jakoby, R., Zierer, T., Lindblad, K., Larsson, J., DeVito, L., Bohn, Dieter E., Funcke, J. and Decker, A. (2004), Numerical Simulation of the Unsteady Flow Field in an Axial Gas Turbine Rim Seal Configuration. *Turbo Expo*, Vol. 4, pp. 431–440, DOI 10.1115/GT2004-53829.
- Schneiders, L., Günther, C., Meinke, M. and Schröder, W. (2016), An efficient conservative cut-cell method for rigid bodies interacting with viscous compressible flows, *Journal of Computational Physics*, Vol. 311, pp. 62–86.